Neurocomputing 73 (2010) 3066–3078

Contents lists available at ScienceDirect

Neurocomputing

journal homepage: www.elsevier.com/locate/neucom

The Bogdanov–Takens bifurcation analysis on a three dimensional recurrent neural network

Farzaneh Maleki [a], Babak Beheshti [a], Amirhossein Hajihosseini [a,*], Gholam Reza Rokni Lamooki [a,b]

[a] Center of Excellence in Biomathematics, School of Mathematics, Statistics and Computer Science, University of Tehran, Tehran 14176-14411, Iran
[b] School of Mathematics, Statistics and Computer Science, College of Science, University of Tehran, Tehran 14176-14411, Iran

ARTICLE INFO

Article history:
Received 9 November 2009
Received in revised form
21 April 2010
Accepted 28 June 2010
Communicated by W. Lu
Available online 27 August 2010

Keywords:
Recurrent neural networks
Bogdanov–Takens bifurcation
Hopf bifurcation
Pitchfork bifurcation
Homoclinic orbit
Heteroclinic orbit

ABSTRACT

A class of recurrent neural networks is investigated in the vicinity of the Bogdanov–Takens bifurcation point in the parameter space when the slope of the transfer function of the neurons at the origin is not equal to one. It will be shown that two different bifurcation diagrams can be constructed. In each bifurcation diagram, there are critical values for the parameters of the network for which curves of pitchfork and Hopf bifurcation intersect each other at a point where the linear part of the system that describes the network, has a pair of simple zero eigenvalues. As curves of homoclinic and heteroclinic bifurcation emanate from the Bogdanov–Takens point, a complicated behavior is observed by the variation of weights in the recurrent neural network.

1. Introduction and problem statement

Recurrent neural networks (RNNs) including Cohen–Grossberg neural networks (CGNNs), Hopfield neural networks (HNNs) and cellular neural networks (CNNs) have been used extensively in different areas such as signal processing, pattern recognition, optimization and associative memories [5,13] in which the stability of equilibrium in the network is widely investigated. They are also one of the best choices for learning input and output data which dynamically vary by time [6,21,31]. One of the main focuses of research on RNNs has always been the existence of periodic solutions and mechanisms under which such solutions emerge. Studies related to the existence of periodic solutions in a certain type of cyclic recurrent neural configurations can be found in [1,8,12]. One of the natural features of recurrent neural networks is the presence of time delays in their dynamical models. Many rich mathematical investigations and results on recurrent neural networks with time delays are available in the literature. These investigations include the global asymptotic and exponential stability of equilibria and also the existence and stability of periodic solutions with and without time delays; see for example [2–4,10,16–19,23–25,27–29] and also [32] for some recent references on RNNs with both constant and time-varying delays. In [11], Haschke et al. have given analytical expressions for bifurcation manifolds in the input space of general discrete-time RNNs for the case of three-neuron networks.

In this paper, we study a three-neuron recurrent neural network in feedback configuration. Ruiz et al. studied this model in [22] for the first time. Fig. 1 illustrates the class of recurrent neural networks that they considered in their investigations. In Fig. 1, $u(t)$ is the input and $y(t)$ is the output of the network. This network can be described by the following system:

$$\begin{cases} \dot{x}_1(t) = -x_1(t) + f(x_2(t)), \\ \vdots \\ \dot{x}_{n-1}(t) = -x_{n-1}(t) + u(t), \\ \dot{x}_n(t) = -x_n(t) + w_1 f(x_1(t)) + \cdots + w_{n-1} f(x_{n-1}(t)), \\ y(t) = f(x_n(t)). \end{cases} \tag{1}$$

Here, $x(t) \in \mathbb{R}^n$ is the state variable, $w_i \in \mathbb{R}$, $i=1,\ldots,n-1$ are the network parameters or weights, $u(t)$ is the input and $y(t)$ is the output. The function $f(\cdot)$ represents the transfer function of the neurons. Ruiz et al. [22] showed that a three-neuron network of the form (1), with $f(\cdot)=\tanh(\cdot)$, has the capability of learning a specific class of time-varying periodic signals. According to [22], system (1) receives the input $u(t)$ as an unknown signal and then after a period of length $T>0$, during which $w_i(t)$, $i=1,\ldots,n-1$ are adapted, with the intention that $y(t)$ tracks $u(t)$, the input $u(t)$ is replaced by the output $y(t)$. The three-node network studied in

* Corresponding author.
E-mail addresses: hajihosseini@khayam.ut.ac.ir, amirhossein80@gmail.com (A. Hajihosseini).

0925-2312/$ - see front matter © 2010 Elsevier B.V. All rights reserved.
doi:10.1016/j.neucom.2010.06.023

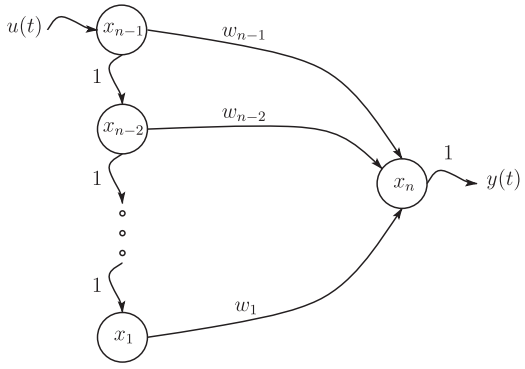

Fig. 1. Class of recurrent neural networks studied in [22].

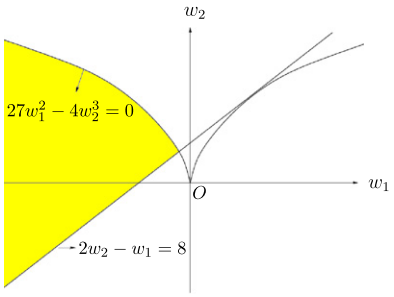

Fig. 2. The bifurcation diagram presented in [22]. In the shaded region, the linearization of system (2) with $f(\cdot)=\tanh(\cdot)$ at the unique equilibrium (0,0,0) has a negative real eigenvalue and a pair of complex conjugate eigenvalues with positive real part.

[22] and [26] in feedback configuration, with $u(t)=y(t)$, is as follows:

$$\begin{cases} \dot{x}_1(t) = -x_1(t)+f(x_2(t)), \\ \dot{x}_2(t) = -x_2(t)+f(x_3(t)), \\ \dot{x}_3(t) = -x_3(t)+w_1 f(x_1(t))+w_2 f(x_2(t)), \end{cases} \tag{2}$$

where $w_1 \in \mathbb{R}$ and $w_2 \in \mathbb{R}$, are fixed. It is important to note that system (2) with $f(\cdot)=\tanh(\cdot)$, is $\mathbb{Z}_2$-symmetric; in other words, it is invariant under the rotation through the angle π; see [15]. Ruiz et al. [22] considered system (2) with the transfer function $f(\cdot)=\tanh(\cdot)$ and proved that in a specific region in the (w_1,w_2)-space determined by inequalities

$$2w_2-w_1 \geq 8 \quad \text{and} \quad 27w_1^2-4w_2^3>0, \tag{3}$$

the linearization of system (2) with $f(\cdot)=\tanh(\cdot)$ at the unique equilibrium (0,0,0) has a negative real eigenvalue and a pair of complex conjugate eigenvalues with positive real part. In particular, they showed that the curve $2w_2-w_1=8$, with $w_1<-2$, is the Hopf bifurcation curve in the two-dimensional parameter space on which the two complex conjugate eigenvalues become purely imaginary. Fig. 2 depicts the bifurcation diagram presented in [22] and also the region (shaded area) determined by inequalities (3). It is easy to check that the linearization of system (2), with $f(\cdot)=\tanh(\cdot)$, at the equilibrium $(x_1^*, x_2^*, x_3^*)=(0,0,0)$ has a pair of simple zero eigenvalues at $(w_1^*, w_2^*)=(-2,3)$ where the two curves $27w_1^2-4w_2^3=0$ and $2w_2-w_1=8$ intersect each other.

Recently, Hajihosseini et al. [10] studied system (2) with distributed delays when $f(\cdot)=\tanh(\cdot)$ is taken as the transfer function of the neurons. By using the strong kernel and applying the Moiola and Chen formulation of the frequency domain [20], it was shown that for a fixed choice of the mean delay as the bifurcation parameter, there are corresponding values of the network parameters w_1 and w_2 for which system (2) undergoes a Hopf bifurcation at the origin. Thereby, even with the presence of time delays, this class of recurrent neural networks was proved to have the capability of learning given periodic signals.

In this paper, we consider system (2) with a general transfer function. We replace $\tanh(\cdot)$ with a function with the Taylor series expansion at the origin of the form

$$f(x)=\sum_{i=1}^{\infty} \alpha_{2i-1} x^{2i-1}, \tag{4}$$

where $\alpha_{2i-1}>0$ for i odd and $\alpha_{2i-1}<0$ for i even. This new transfer function still preserves the same properties of oddity, continuity, monotonicity and smoothness and is assumed to be bounded. If we take $\tanh(\cdot)$ as the transfer function, Eq. (4) will represent the Taylor expansion of this function with $\alpha_1=1$, $\alpha_3=-1/3$, etc. System (2) with transfer function (4) is a $\mathbb{Z}_2-$symmetric system. By using Eq. (4) as the transfer function of the neurons, we investigate a broader class of periodic signals that networks of the form (2) can learn. Our investigation improves and broadens previous results in [7,10,22] and shows that when $\alpha_1=1$, some results in [7] are not generic.

Recently, Gao et al. [7] studied system (2) with $f(\cdot)=\tanh(\cdot)$ and obtained a single equation for the equilibria of this system by using the iterates of the transcendental transfer function, $\tanh(\cdot)$. They showed that in a specific region in the bifurcation diagram in Fig. 2, the number of equilibria of system (2) changes from one to five. This region is determined by inequalities

$$27w_1^2-4w_2^3<0 \quad \text{and} \quad w_1+w_2<1 \quad \text{and} \quad w_2>3. \tag{5}$$

Based on their studies on the equilibria of system (2), Gao et al. [7] introduced two bifurcation curves in the region determined by inequalities (5). These curves include a saddle-node and a Hopf bifurcation curve. The two curves are illustrated in Fig. 3. The saddle-node and the Hopf bifurcation curves are labeled with S and H, respectively.

We analyze system (2) with transfer function (4) in the neighborhood of the Bogdanov–Takens codimension two bifurcation point in the (w_1,w_2)-space. We will show that if $\alpha_1 \neq 1$ in transfer function (4), system (2) can be reduced to the following system:

$$\begin{cases} \dot{x}_1(t) = x_2(t), \\ \dot{x}_2(t) = \mu_1 x_1(t)+\mu_2 x_2(t)+a_3 x_1^3(t)+b_3 x_1^2(t)x_2(t), \end{cases} \tag{6}$$

where μ_1 and μ_2 are the unfolding parameters and are functions of w_1, w_2 and α_1. System (6) has at most three equilibria and does not undergo the saddle-node and the Hopf bifurcation in the region determined by inequalities (5). In other words, the two bifurcation curves, labeled with S and H in Fig. 3, vanish when $\alpha_1 \neq 1$; as a result, their presence in the parameter space is not generic for systems with $\mathbb{Z}_2$-symmetry. In addition, we will show

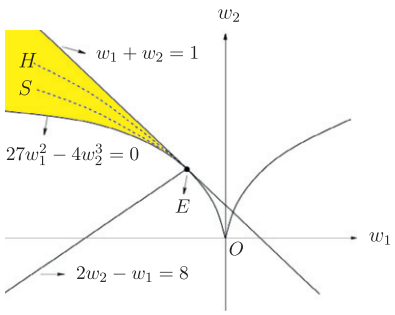

Fig. 3. The bifurcation diagram presented in [7]. The shaded region is determined by inequalities (5). The two dashed curves S and H in the shaded region, represent the saddle-node and the Hopf bifurcation curves, respectively. The point $E(-2,3)$ denotes the Bogdanov–Takens bifurcation point in the parameter space.

that there are other bifurcation curves along with the Hopf bifurcation curve in the parameter space emanating from the Bogdanov–Takens point. These include a curve of pitchfork, homoclinic and heteroclinic bifurcation and a fold bifurcation curve for limit cycles.

This paper is organized as follows. In Section 2, we first reduce the original system to the center manifold corresponding to a pair of simple zero eigenvalues. Then by applying appropriate change of variables, we obtain the normal form of the system at the bifurcation point and introduce the unfolding parameters. In Section 3, a full investigation is carried out on the reduced system in the vicinity of the bifurcation point, and all possible bifurcations that take place in this system, are analyzed. In Section 4, bifurcation diagrams for different choices of a_3, according to its sign, are presented. By using the parameter values in different regions, determined by the bifurcation curves, several phase portraits of the system are constructed.

2. Center manifold reduction and the normal form

Consider system (2) with transfer function (4). Thus,

$$\begin{cases} \dot{x}_1(t) = -x_1(t) + \alpha_1 x_2 + \alpha_3 x_2^3 + \mathcal{O}(x_2^5), \\ \dot{x}_2(t) = -x_2(t) + \alpha_1 x_3 + \alpha_3 x_3^3 + \mathcal{O}(x_3^5), \\ \dot{x}_3(t) = -x_3(t) + w_1(\alpha_1 x_1 + \alpha_3 x_1^3 + \mathcal{O}(x_1^5)) \\ \qquad + w_2(\alpha_1 x_2 + \alpha_3 x_2^3 + \mathcal{O}(x_2^5)). \end{cases} \tag{7}$$

Linearization of system (7) at the equilibrium $(x_1^*, x_2^*, x_3^*)=(0,0,0)$ is given by

$$J(w_1,w_2) = \begin{pmatrix} -1 & \alpha_1 & 0 \\ 0 & -1 & \alpha_1 \\ \alpha_1 w_1 & \alpha_1 w_2 & -1 \end{pmatrix}, \tag{8}$$

with the characteristic equation

$$\lambda^3 + 3\lambda^2 + (3-\alpha_1^2 w_2)\lambda + (1-\alpha_1^2 w_2 - \alpha_1^3 w_1) = 0. \tag{9}$$

According to Eq. (9), if we set $w_1 = w_1^* = -2/\alpha_1^3$ and $w_2 = w_2^* = 3/\alpha_1^2$, the roots of Eq. (9) will be $\lambda_1 = 0, \lambda_2 = 0$ and $\lambda_3 = -3$. In other words, at $(w_1^*, w_2^*) = (-2/\alpha_1^3, 3/\alpha_1^2)$, the linearized system has a pair of simple zero eigenvalues. We will study system (2) in the neighborhood of the point (w_1^*, w_2^*) in the (w_1, w_2)-space. To this end, we need to reduce system (7) to the center manifold corresponding to this pair of simple zero eigenvalues. For this, we consider the following transformations:

$$\begin{pmatrix} x_1 \\ x_2 \\ x_3 \end{pmatrix} = \begin{pmatrix} \alpha_1^2 & 0 & \frac{1}{4}\alpha_1^2 \\ \alpha_1 & \alpha_1 & -\frac{1}{2}\alpha_1 \\ 1 & 2 & 1 \end{pmatrix} \begin{pmatrix} y_1 \\ y_2 \\ y_3 \end{pmatrix}, \tag{10}$$

$$\begin{pmatrix} y_1 \\ y_2 \\ y_3 \end{pmatrix} = \frac{1}{9\alpha_1^2} \begin{pmatrix} 8 & 2\alpha_1 & -\alpha_1^2 \\ -6 & 3\alpha_1 & 3\alpha_1^2 \\ 4 & -8\alpha_1 & 4\alpha_1^2 \end{pmatrix} \begin{pmatrix} x_1 \\ x_2 \\ x_3 \end{pmatrix}. \tag{11}$$

Using transformations (10) and (11), we put system (7) into the standard form

$$\begin{pmatrix} \dot{y}_1 \\ \dot{y}_2 \\ \dot{y}_3 \end{pmatrix} = \begin{pmatrix} 0 & 1 & 0 \\ 0 & 0 & 0 \\ 0 & 0 & -3 \end{pmatrix} \begin{pmatrix} y_1 \\ y_2 \\ y_3 \end{pmatrix} + \begin{pmatrix} F_1(y_1,y_2,y_3) \\ F_2(y_1,y_2,y_3) \\ F_3(y_1,y_2,y_3) \end{pmatrix}, \tag{12}$$

where

$$\begin{aligned} F_1(y_1,y_2,y_3) = {} & a_{300}y_1^3 + a_{210}y_1^2y_2 + a_{120}y_1y_2^2 \\ & + a_{030}y_2^3 + a_{201}y_1^2y_3 + a_{102}y_1y_3^2 + a_{021}y_2^2y_3 \\ & + a_{012}y_2y_3^2 + a_{003}y_3^3 + a_{111}y_1y_2y_3 + \mathcal{O}(|(y_1,y_2,y_3)|^5), \end{aligned}$$

and

$$\begin{aligned} F_2(y_1,y_2,y_3) = {} & b_{300}y_1^3 + b_{210}y_1^2y_2 + b_{120}y_1y_2^2 + b_{030}y_2^3 \\ & + b_{201}y_1^2y_3 + b_{102}y_1y_3^2 + b_{021}y_2^2y_3 + b_{012}y_2y_3^2 \\ & + b_{003}y_3^3 + b_{111}y_1y_2y_3 + \mathcal{O}(|(y_1,y_2,y_3)|^5), \end{aligned}$$

and

$$\begin{aligned} F_3(y_1,y_2,y_3) = {} & c_{300}y_1^3 + c_{210}y_1^2y_2 + c_{120}y_1y_2^2 + c_{030}y_2^3 \\ & + c_{201}y_1^2y_3 + c_{102}y_1y_3^2 + c_{021}y_2^2y_3 + c_{012}y_2y_3^2 + c_{003}y_3^3 \\ & + c_{111}y_1y_2y_3 + \mathcal{O}(|(y_1,y_2,y_3)|^5), \end{aligned}$$

where

$$a_{300} = \frac{\alpha_3}{9\alpha_1}(2+5\alpha_1^2+2\alpha_1^4), \quad a_{210} = \frac{\alpha_3}{3\alpha_1}(4+5\alpha_1^2),$$
$$a_{120} = \frac{\alpha_3}{3\alpha_1}(8+5\alpha_1^2),$$

$$a_{030} = \frac{\alpha_3}{9\alpha_1}(16+5\alpha_1^2), \quad a_{201} = \frac{\alpha_3}{6\alpha_1}(4-5\alpha_1^2+\alpha_1^4),$$
$$a_{111} = -\frac{\alpha_3}{3\alpha_1}(-8+5\alpha_1^2),$$

$$a_{012} = \frac{\alpha_3}{12\alpha_1}(16+5\alpha_1^2), \quad a_{003} = \frac{\alpha_3}{288\alpha_1}(64-20\alpha_1^2+\alpha_1^4),$$

$$a_{021} = -\frac{\alpha_3}{6\alpha_1}(-16+5\alpha_1^2), \quad a_{102} = \frac{\alpha_3}{24\alpha_1}(16+10\alpha_1^2+\alpha_1^4),$$

and

$$b_{300} = -\frac{\alpha_3}{3\alpha_1}(-1-\alpha_1^2+2\alpha_1^4), \quad b_{210} = \frac{\alpha_3}{\alpha_1}(2+\alpha_1^2), \quad b_{120} = \frac{\alpha_3}{\alpha_1}(4+\alpha_1^2),$$

$$b_{030} = \frac{\alpha_3}{3\alpha_1}(8+\alpha_1^2), \quad b_{201} = -\frac{\alpha_3}{2\alpha_1}(-2+\alpha_1^2+\alpha_1^4),$$
$$b_{111} = -\frac{\alpha_3}{\alpha_1}(-4+\alpha_1^2),$$

$$b_{012} = \frac{\alpha_3}{4\alpha_1}(8+\alpha_1^2), \quad b_{003} = -\frac{\alpha_3}{96\alpha_1}(-32+4\alpha_1^2+\alpha_1^4),$$

$$b_{021} = -\frac{\alpha_3}{2\alpha_1}(-8+\alpha_1^2), \quad b_{102} = -\frac{\alpha_3}{8\alpha_1}(-8-2\alpha_1^2+\alpha_1^4),$$

and

$$c_{300} = -\frac{8\alpha_3}{9\alpha_1}(1-2\alpha_1^2+\alpha_1^4), \quad c_{210} = \frac{16\alpha_3}{3\alpha_1}(-1+\alpha_1^2),$$
$$c_{120} = \frac{16\alpha_3}{3\alpha_1}(-2+\alpha_1^2),$$

$$c_{030} = \frac{16\alpha_3}{9\alpha_1}(-4+\alpha_1^2), \quad c_{201} = -\frac{2\alpha_3}{3\alpha_1}(4+4\alpha_1^2+\alpha_1^4),$$
$$c_{111} = -\frac{16\alpha_3}{3\alpha_1}(2+\alpha_1^2),$$

$$c_{012} = \frac{4\alpha_3}{3\alpha_1}(-4+\alpha_1^2), \quad c_{003} = -\frac{\alpha_3}{72\alpha_1}(64+16\alpha_1^2+\alpha_1^4),$$

$$c_{021} = -\frac{8\alpha_3}{3\alpha_1}(4+\alpha_1^2), \quad c_{102} = -\frac{\alpha_3}{6\alpha_1}(16-8\alpha_1^2+\alpha_1^4).$$

We reduce system (12) to a two-dimensional center manifold which corresponds to the pair of simple zero eigenvalues. Since the stable eigenspace (E^s) is one-dimensional, the center manifold is of the form $y_3 = h(y_1,y_2)$; see [9,14,15,30] for more details on center manifold theorem. It can easily be seen that the coefficients of the second order terms in the center manifold are zero. Therefore, we consider the center manifold

$$y_3 = h(y_1,y_2) = ay_1^3 + by_1^2y_2 + cy_1y_2^2 + dy_2^3 + \mathcal{O}(|(y_1,y_2)|^5). \tag{13}$$

By putting the center manifold (13) into the third equation of (12) and then by equating powers of y_1^3, $y_1^2\,y_2$, $y_1y_2^2$ and y_2^3 on both

sides, we can calculate the coefficients of the center manifold as follows:

$$a=-\frac{8\alpha_3}{27\alpha_1}(-2\alpha_1^2+\alpha_1^4+1),\quad b=\frac{8\alpha_3}{27\alpha_1}(4\alpha_1^2+\alpha_1^4-5),$$

$$c=-\frac{16\alpha_3}{81\alpha_1}(-5\alpha_1^2+\alpha_1^4+13),\quad d=\frac{16\alpha_3}{243\alpha_1}(4\alpha_1^2+\alpha_1^4-23).$$

Therefore, system (12) is reduced to the following system:

$$\begin{cases}\dot{y}_1=y_2+\beta_{30}y_1^3+\beta_{21}y_1^2y_2+\beta_{12}y_1y_2^2+\beta_{03}y_2^3+\mathcal{O}(|(y_1,y_2)|^5),\\ \dot{y}_2=\sigma_{30}y_1^3+\sigma_{21}y_1^2y_2+\sigma_{12}y_1y_2^2+\sigma_{03}y_2^3+\mathcal{O}(|(y_1,y_2)|^5),\end{cases}\tag{14}$$

where

$$\beta_{30}=\frac{\alpha_3}{9\alpha_1}(5\alpha_1^2+2\alpha_1^4+2),\quad \beta_{21}=\frac{\alpha_3}{3\alpha_1}(5\alpha_1^2+4),$$

$$\beta_{12}=\frac{\alpha_3}{3\alpha_1}(5\alpha_1^2+8),\quad \beta_{03}=\frac{\alpha_3}{9\alpha_1}(5\alpha_1^2+16),$$

and

$$\sigma_{30}=-\frac{\alpha_3}{3\alpha_1}(-\alpha_1^2+2\alpha_1^4-1),\quad \sigma_{21}=\frac{\alpha_3}{\alpha_1}(\alpha_1^2+2),$$

$$\sigma_{12}=\frac{\alpha_3}{\alpha_1}(\alpha_1^2+4),\quad \sigma_{03}=\frac{\alpha_3}{3\alpha_1}(\alpha_1^2+8).$$

Now, according to [15], we introduce the new variables (u_1,u_2) by

$$\begin{cases}u_1=y_1,\\ u_2=\tilde{F}_1(y_1,y_2),\end{cases}\tag{15}$$

where

$$\tilde{F}_1(y_1,y_2)=y_2+\beta_{30}y_1^3+\beta_{21}y_1^2y_2+\beta_{12}y_1y_2^2+\beta_{03}y_2^3+\mathcal{O}(|(y_1,y_2)|^5).$$

Transformation (15) brings system (14) into

$$\begin{cases}\dot{u}_1=u_2,\\ \dot{u}_2=h_{30}u_1^3+h_{21}u_1^2u_2+h_{12}u_1u_2^2+h_{03}u_2^3+\mathcal{O}(|(u_1,u_2)|^5),\end{cases}\tag{16}$$

where

$$h_{30}=-\frac{\alpha_3}{3\alpha_1}(-\alpha_1^2+2\alpha_1^4-1),\quad h_{12}=\frac{\alpha_3}{3\alpha_1}(13\alpha_1^2+20),$$

$$h_{21}=\frac{2\alpha_3}{3\alpha_1}(4\alpha_1^2+\alpha_1^4+4),\quad h_{03}=\frac{2\alpha_3}{3\alpha_1}(3\alpha_1^2+8).$$

System (16) can be rewritten as

$$\dot{U}=J_{BT}U+G_3(U)+\mathcal{O}(|U|^5),\tag{17}$$

where

$$U=\begin{pmatrix}u_1\\ u_2\end{pmatrix},\quad J_{BT}=\begin{pmatrix}0&1\\0&0\end{pmatrix},$$

$$G_3(U)=\begin{pmatrix}0\\ h_{30}u_1^3+h_{21}u_1^2u_2+h_{12}u_1u_2^2+h_{03}u_2^3\end{pmatrix}.$$

To simplify the third order terms in system (17), we consider the change of coordinates introduced in [9,30]; that is,

$$U=V+H(V),\tag{18}$$

where

$$V=\begin{pmatrix}v_1\\ v_2\end{pmatrix},\quad H(V)=\begin{pmatrix}f_{30}v_1^3+f_{21}v_1^2v_2+f_{12}v_1v_2^2+f_{03}v_2^3\\ g_{30}v_1^3+g_{21}v_1^2v_2+g_{12}v_1v_2^2+g_{03}v_2^3\end{pmatrix},$$

with

$$f_{30}=\frac{\alpha_3}{18\alpha_1}(13\alpha_1^2+20),\quad f_{21}=\frac{\alpha_3}{3\alpha_1}(3\alpha_1^2+8),$$

$$g_{21}=\frac{\alpha_3}{6\alpha_1}(13\alpha_1^2+20),\quad g_{12}=\frac{2\alpha_3}{3\alpha_1}(3\alpha_1^2+8),$$

and $f_{12}=f_{03}=g_{30}=g_{03}=0$. Transformation (18) puts system (17) into the following system:

$$\begin{cases}\dot{v}_1=v_2+\mathcal{O}(|(v_1,v_2)|^5),\\ \dot{v}_2=a_3v_1^3+b_3v_1^2v_2+\mathcal{O}(|(v_1,v_2)|^5),\end{cases}\tag{19}$$

where

$$a_3=-\frac{\alpha_3}{3\alpha_1}(2\alpha_1^4-\alpha_1^2-1),\quad b_3=\frac{2\alpha_3}{3\alpha_1}(\alpha_1^4+4\alpha_1^2+4).$$

In system (19), the coefficient a_3 will be nonzero if $\alpha_1\neq 1$. According to [9,15,30], the higher order terms can be omitted in system (19) due to the structural stability; therefore, the following system will be taken into account:

$$\begin{cases}\dot{v}_1=v_2,\\ \dot{v}_2=a_3v_1^3+b_3v_1^2v_2.\end{cases}\tag{20}$$

System (20) represents the normal form of system (7) at the Bogdanov–Takens bifurcation point where $(w_1^*,w_2^*)=(-2/\alpha_1^3,3/\alpha_1^2)$. Since $\alpha_1>0$ and $\alpha_3<0$, b_3 is always negative. If $\alpha_1<1$, then $a_3<0$ and if $\alpha_1>1$, then $a_3>0$. In the case of $\alpha_1=1$, the nondegeneracy condition of the Bogdanov–Takens bifurcation, that is $a_3\neq 0$, will be violated and therefore we need to consider higher order terms in the normal form of the system at the Bogdanov–Takens bifurcation point. By using $\tanh(\cdot)$ as the transfer function of the neurons, Gao et al. [7] have shown the existence of two bifurcation curves in a specific region in the parameter space determined by inequalities (5); see Fig. 3. By using the normal form (20), one can study system (7) in the neighborhood of the Bogdanov–Takens bifurcation point in the parameter space and show that those two bifurcation curves vanish when α_1 takes positive values other than one.

Now, if we repeat the same procedure of reducing to center manifold and applying the change of coordinates (15) and (18) in the vicinity of (w_1^*, w_2^*) for $\alpha_1\neq 1$, we will obtain the normal form whose coefficients are functions of w_1 and w_2. Thus, the unfolding terms will automatically emerge. Therefore, system (7) takes the form

$$\begin{cases}\dot{v}_1=v_2,\\ \dot{v}_2=\mu_1(w_1,w_2)v_1+\mu_2(w_1,w_2)v_2+\tilde{a}_3(w_1,w_2)v_1^3+\tilde{b}_3(w_1,w_2)v_1^2v_2,\end{cases}\tag{21}$$

with

$$\mu_1(w_1,w_2)=\frac{1}{3}(w_1\alpha_1^3+w_2\alpha_1^2-1),$$

$$\mu_2(w_1,w_2)=\frac{1}{9}(-w_1\alpha_1^3+2w_2\alpha_1^2-8),\tag{22}$$

and

$$\mu_1(w_1^*,w_2^*)=\mu_2(w_1^*,w_2^*)=0,\quad \tilde{a}_3(w_1^*,w_2^*)=a_3,\quad \tilde{b}_3(w_1^*,w_2^*)=b_3.\tag{23}$$

Since we have applied the change of coordinates (10), (11), (15) and (18) in a small neighborhood of (w_1^*, w_2^*), the coefficients $\tilde{a}_3$ and $\tilde{b}_3$ preserve the sign of a_3 and b_3 due to their continuous dependence on parameters. By introducing the change of variables and rescaling of time

$$\xi_1=\frac{\tilde{b}_3}{\sqrt{|\tilde{a}_3|}}v_1,\quad \xi_2=-\frac{\tilde{b}_3^2}{|\tilde{a}_3|\sqrt{|\tilde{a}_3|}}v_2,\quad \tau=-\frac{|\tilde{a}_3|}{\tilde{b}_3}t,\tag{24}$$

system (21) becomes

$$\begin{cases} \dot{\xi}_1 = \xi_2, \\ \dot{\xi}_2 = \tilde{\mu}_1\xi_1 + \tilde{\mu}_2\xi_2 + s\xi_1^3 - \xi_1^2\xi_2, \end{cases} \tag{25}$$

where $s = \mathrm{sgn}(\tilde{a}_3)$, and

$$\tilde{\mu}_1 = \tilde{\mu}_1(w_1,w_2) = \left(\frac{\tilde{a}_3}{\tilde{b}_3}\right)^2 \mu_1(w_1,w_2),$$
$$\tilde{\mu}_2 = \tilde{\mu}_2(w_1,w_2) = -\frac{|\tilde{a}_3|}{\tilde{b}_3}\mu_2(w_1,w_2). \tag{26}$$

By using system (25), we can study the qualitative behavior of the original system (7) in the neighborhood of the Bogdanov–Takens codimension two bifurcation point, $(x_1^*,x_2^*,x_3^*,w_1^*,w_2^*) = (0,0,0,-2/\alpha_1^3,3/\alpha_1^2)$, and study all possible codimension one bifurcations and obtain their corresponding curves in the (w_1,w_2)-space.

3. Bifurcation analysis

The equilibria of system (25) are given by

$$\xi_2 = 0 \quad \text{and} \quad \tilde{\mu}_1\xi_1 + s\xi_1^3 = 0. \tag{27}$$

Therefore, one obtains

$$E_1(s) = (0,0) \quad \text{and} \quad E_{2,3}(s) = \left(\mp\sqrt{-\frac{\tilde{\mu}_1}{s}},0\right). \tag{28}$$

The point $E_1(s)$ is always an equilibrium of system (25), but the existence of the two equilibria $E_{2,3}(s)$ depends on the sign of both s and $\tilde{\mu}_1$. In what follows, we consider system (25) in two different cases $s=1$ and -1, and investigate all possible bifurcations that take place in the system. According to Eqs. (26), we can express $\tilde{\mu}_1$ and $\tilde{\mu}_2$ in terms of μ_1 and μ_2 with which we can achieve the equations for the bifurcation curves in the (w_1,w_2)-space by using Eqs. (22).

3.1. The case $s=1$

In this case, the equilibria (28) take the following form:

$$E_1(1) = (0,0) \quad \text{and} \quad E_{2,3}(1) = (\mp\sqrt{-\tilde{\mu}_1},0). \tag{29}$$

It is clear that the two equilibria $E_{2,3}(1)$ vanish when $\tilde{\mu}_1 > 0$. This implies that the curve $\tilde{\mu}_1 = 0$ can be taken as a pitchfork bifurcation curve in the (w_1,w_2)-space on which the two equilibria $E_{2,3}(1)$ collide with each other at the equilibrium $E_1(1)$ and as a result, the origin will be the only equilibrium of system (25). To study system (25) around the curve $\tilde{\mu}_1 = 0$, we consider the linearization of system (25) at $E_1(1)$; that is,

$$J[E_1(1)] = \begin{pmatrix} 0 & 1 \\ \tilde{\mu}_1 & \tilde{\mu}_2 \end{pmatrix}. \tag{30}$$

In the Jacobian matrix (30), if we put $\tilde{\mu}_1 = 0$, the eigenvalues will be $\lambda_1 = 0$ and $\lambda_2 = \tilde{\mu}_2$ when $\tilde{\mu}_2 \neq 0$. We can reduce system (25) to the center manifold corresponding to the zero eigenvalue. To this end, we have to first put the system into its standard form. For this, we apply the following change of coordinates for small $|\tilde{\mu}_1|$

$$\begin{pmatrix} \xi_1 \\ \xi_2 \end{pmatrix} = \begin{pmatrix} 1 & 1 \\ 0 & \tilde{\mu}_2 \end{pmatrix}\begin{pmatrix} z_1 \\ z_2 \end{pmatrix}, \tag{31}$$

$$\begin{pmatrix} z_1 \\ z_2 \end{pmatrix} = \begin{pmatrix} 1 & -1/\tilde{\mu}_2 \\ 0 & 1/\tilde{\mu}_2 \end{pmatrix}\begin{pmatrix} \xi_1 \\ \xi_2 \end{pmatrix}. \tag{32}$$

Then the standard form of system (25) will be given by

$$\begin{cases} \dot{z}_1 = -\dfrac{1}{\tilde{\mu}_2}(\tilde{\mu}_1 z_1 + \tilde{\mu}_1 z_2 + z_1^3 + (3-\tilde{\mu}_2)z_1^2 z_2 + (3-2\tilde{\mu}_2)z_1 z_2^2 \\ \qquad\qquad + (1-\tilde{\mu}_2)z_2^3), \\ \dot{z}_2 = \dfrac{1}{\tilde{\mu}_2}(\tilde{\mu}_1 z_1 + (\tilde{\mu}_1 + \tilde{\mu}_2^2)z_2 + z_1^3 + (3-\tilde{\mu}_2)z_1^2 z_2 + (3-2\tilde{\mu}_2)z_1 z_2^2 \\ \qquad\qquad + (1-\tilde{\mu}_2)z_2^3). \end{cases} \tag{33}$$

Since the coefficient of z_1^3 in the first equation of system (33) is nonzero, we can consider the trivial center manifold $z_2 = h(z_1) = 0$; see [15] for more details. The reduced system then takes the following form:

$$\dot{z}_1 = N(z_1,\tilde{\mu}_1) = -\frac{1}{\tilde{\mu}_2}(\tilde{\mu}_1 z_1 + z_1^3). \tag{34}$$

It is easy to check that genericity conditions hold for the pitchfork bifurcation [15]; that is, transversality and nondegeneracy conditions

$$\left.\frac{\partial^3 N}{\partial z_1^3}(z_1,\tilde{\mu}_1)\right|_{z_1=0,\tilde{\mu}_1=0} = -\frac{6}{\tilde{\mu}_2} \neq 0, \quad \left.\frac{\partial^2 N}{\partial z_1 \tilde{\mu}_1}(z_1,\tilde{\mu}_1)\right|_{z_1=0,\tilde{\mu}_1=0} = -\frac{1}{\tilde{\mu}_2} \neq 0. \tag{35}$$

Conditions (35) state that a generic pitchfork bifurcation takes place in system (25) at the equilibrium $E_1(1)$ as the parameter $\tilde{\mu}_1$ passes zero. In other words, in the (w_1,w_2)-space when $\tilde{\mu}_2 \neq 0$, system (25) undergoes a generic pitchfork bifurcation on the curve $\tilde{\mu}_1 = 0$.

Consider the Jacobian matrix (30) again. If $\tilde{\mu}_2 = 0$ and $\tilde{\mu}_1 < 0$, the linear part of system (25) will have a pair of purely imaginary eigenvalues; this is the necessary condition for the Hopf bifurcation. In order to show that a generic Hopf bifurcation takes place in system (25) and also to find its direction, we need to focus our attention on the genericity conditions again, this time for the Hopf bifurcation [15]; that is,

$$\frac{d}{d\tilde{\mu}_2} Re\lambda_{1,2}(\tilde{\mu}_2)\Big|_{\tilde{\mu}_2=0} \neq 0 \quad \text{and} \quad Re[c_1(\tilde{\mu}_2)]|_{\tilde{\mu}_2=0} \neq 0, \tag{36}$$

where

$$\lambda_{1,2} = \frac{\tilde{\mu}_2 \pm \sqrt{\tilde{\mu}_2^2 + 4\tilde{\mu}_1}}{2},$$

and $Re[c_1(\cdot)]$ is the leading coefficient in the normal form of the Hopf bifurcation. The transversality condition holds, because it can easily be shown that

$$\frac{d}{d\tilde{\mu}_2} Re\lambda_{1,2}(\tilde{\mu}_2)\Big|_{\tilde{\mu}_2=0} = \frac{1}{2} \neq 0. \tag{37}$$

For calculating $Re[c_1(\tilde{\mu}_2)]$ at $\tilde{\mu}_2 = 0$, we need to put system (25) into its standard form. Under the change of coordinates

$$\begin{pmatrix} \xi_1 \\ \xi_2 \end{pmatrix} = \begin{pmatrix} 0 & 1 \\ \sqrt{-\tilde{\mu}_1} & 0 \end{pmatrix}\begin{pmatrix} z_1 \\ z_2 \end{pmatrix}, \tag{38}$$

$$\begin{pmatrix} z_1 \\ z_2 \end{pmatrix} = \begin{pmatrix} 0 & 1/\sqrt{-\tilde{\mu}_1} \\ 1 & 0 \end{pmatrix}\begin{pmatrix} \xi_1 \\ \xi_2 \end{pmatrix}, \tag{39}$$

for small $|\tilde{\mu}_2|$, system (25) will be brought into

$$\begin{cases} \dot{z}_1 = \tilde{\mu}_2 z_1 + \dfrac{\tilde{\mu}_1}{\sqrt{-\tilde{\mu}_1}} z_2 - z_1 z_2^2 + \dfrac{1}{\sqrt{-\tilde{\mu}_1}} z_2^3, \\ \dot{z}_2 = \sqrt{-\tilde{\mu}_1} z_1. \end{cases} \tag{40}$$

Now, by using the stability formula [9]

$$Re[c_1(\tilde{\mu}_2)]|_{\tilde{\mu}_2=0} = \frac{1}{16}[F_{z_1z_1z_1} + F_{z_1z_2z_2} + G_{z_1z_1z_2} + G_{z_2z_2z_2}]$$

$$+\frac{1}{16\omega}[F_{z_1z_2}(F_{z_1z_1}+F_{z_2z_2})-G_{z_1z_2}(G_{z_1z_1}+G_{z_2z_2}) -F_{z_1z_1}G_{z_1z_1}+F_{z_2z_2}G_{z_2z_2}], \quad (41)$$

for

$$F=-z_1z_2^2+\frac{1}{\sqrt{-\tilde{\mu}_1}}z_2^3, \quad G=0, \quad \text{and} \quad \omega=\sqrt{-\tilde{\mu}_1}, \quad (42)$$

one obtains

$$Re[c_1(\tilde{\mu}_2)]|_{\tilde{\mu}_2=0}=-\frac{1}{8}<0. \quad (43)$$

Inequality (43) indicates that the Hopf bifurcation is supercritical; that is, a family of stable periodic solutions emerge as the bifurcation parameter, $\tilde{\mu}_2$, passes its critical value, zero. In other words, system (25) undergoes a generic supercritical Hopf bifurcation at $E_1(1)$ on the curve $\tilde{\mu}_2=0$. In addition, when $\tilde{\mu}_1>0$, the origin is a saddle. We already know that the two equilibria $E_2(1)$ and $E_3(1)$ will exist if $\tilde{\mu}_1<0$. The linearization of system (25) at these two equilibria is given by

$$J[E_{2,3}(1)]=\begin{pmatrix}0 & 1\\ -2\tilde{\mu}_1 & \tilde{\mu}_1+\tilde{\mu}_2\end{pmatrix}. \quad (44)$$

Since $\tilde{\mu}_1<0$, $detJ[E_{2,3}(1)]<0$. Thus, both equilibria $E_2(1)$ and $E_3(1)$ are saddles.

According to [9], there is a curve of heteroclinic bifurcation given by the following equation:

$$\tilde{\mu}_2=-\frac{1}{5}\tilde{\mu}_1+\mathcal{O}(\tilde{\mu}_1^2). \quad (45)$$

On this curve, two heteroclinic orbits will emerge to connect the two equilibria $E_2(1)$ and $E_3(1)$ through their stable and unstable manifolds.

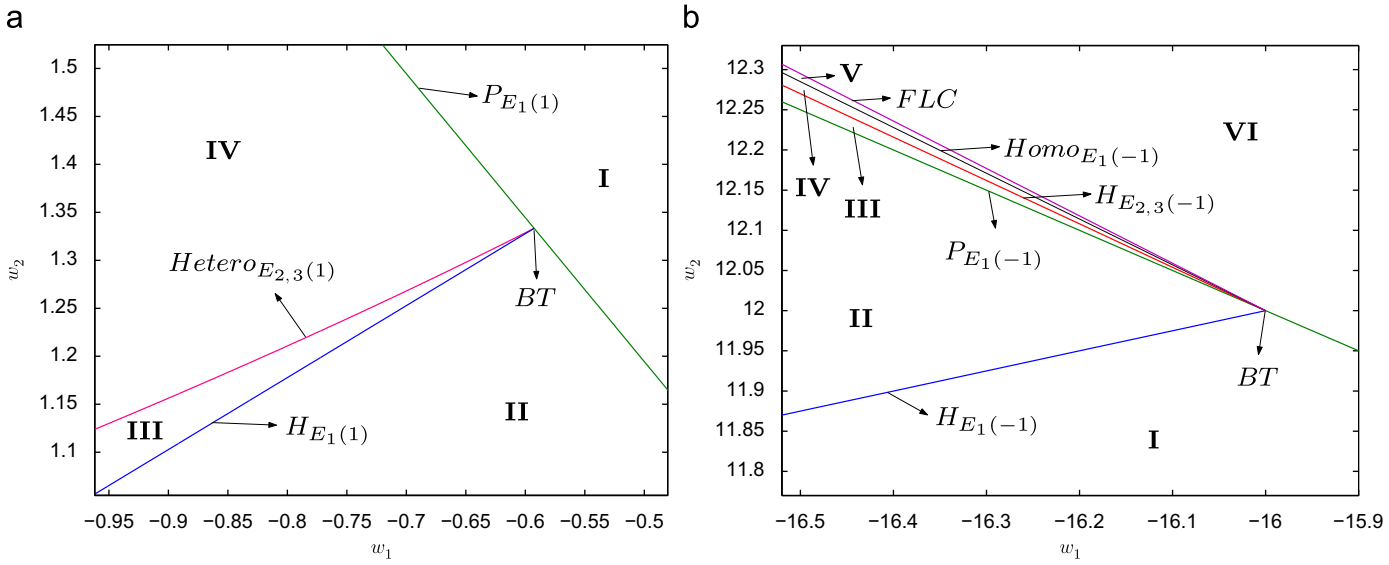

Fig. 4. Bifurcation diagrams of system (7). (a) When $s=1$ and $f(\cdot)=\frac{3}{2}\tanh(\cdot)$ is taken as the transfer function of the neurons. The pitchfork and Hopf (at $E_1(1)$) and heteroclinic bifurcation curves are labeled with $P_{E_1(1)}$, $H_{E_1(1)}$ and $Hetero_{E_{2,3}(1)}$, respectively. (b) When $s=-1$ and $f(\cdot)=\frac{1}{2}\tanh(\cdot)$ is taken as the transfer function of the neurons. The pitchfork and Hopf (at $E_1(-1)$), Hopf (at $E_2(-1)$ and $E_3(-1)$) and homoclinic bifurcation curves, and the curve of fold bifurcation for limit cycles are labeled with $P_{E_1(-1)}$, $H_{E_1(-1)}$, $H_{E_{2,3}(-1)}$, $Homo_{E_1(-1)}$ and FLC, respectively.

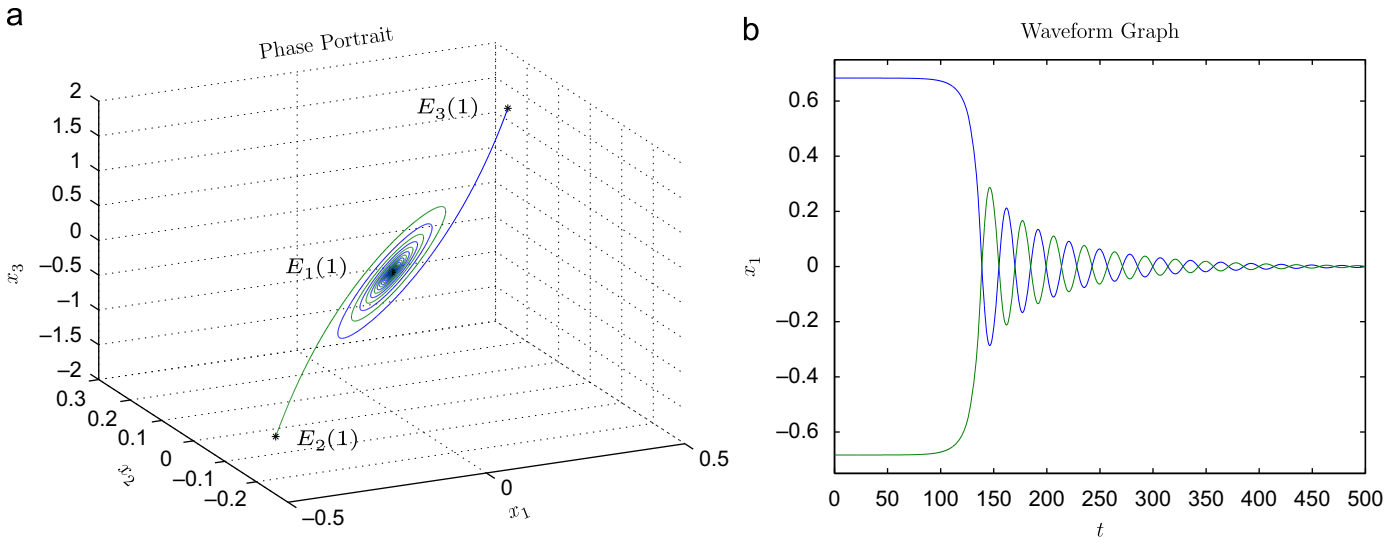

Fig. 5. Numerical results for system (7) in region (II) of Fig. 4a when $(w_1,w_2)=(-0.6,1.28)$. In this region, the equilibrium $E_1(1)$ becomes stable and two nonzero saddles appear. The phase portrait (a) and its corresponding waveform graph (b) show that the unstable manifolds of $E_2(1)$ and $E_3(1)$ are attracted by $E_1(1)$.

3.2. The case $s=-1$

In this case, the equilibria (28) become

$$E_1(-1)=(0,0) \quad \text{and} \quad E_{2,3}(-1)=(\mp\sqrt{\tilde{\mu}_1},0). \tag{46}$$

The linearization of system (25) at $E_1(-1)$ is the same as the Jacobian matrix (30) and therefore, similar to the previous case, system (25) undergoes a pitchfork bifurcation on the curve $\tilde{\mu}_1=0$ when $\tilde{\mu}_2\neq 0$ and a Hopf bifurcation on $\tilde{\mu}_2=0$ when $\tilde{\mu}_1<0$. The genericity conditions can similarly be shown for both bifurcations.

Consider the situation when system (25) has three equilibria, that is when $\tilde{\mu}_1>0$. The Jacobian matrix of system (25) at $E_{2,3}(-1)$ is then given by

$$J[E_{2,3}(-1)]=\begin{pmatrix} 0 & 1 \\ -2\tilde{\mu}_1 & \tilde{\mu}_2-\tilde{\mu}_1 \end{pmatrix}. \tag{47}$$

The Jacobian matrix (47) has a pair of purely imaginary eigenvalues when $\tilde{\mu}_2=\tilde{\mu}_1$. To show that system (25) generically undergoes a Hopf bifurcation at the two nonzero equilibria $E_2(-1)$ and $E_3(-1)$, we consider the same procedure to calculate conditions (36) at $\tilde{\mu}_2=\tilde{\mu}_1$. Here, we show the genericity conditions only for $E_3(-1)=(\sqrt{\tilde{\mu}_1},0)$. Similar results can be achieved for $E_2(-1)$. Consider the following change of variables:

$$(\xi_1,\xi_2)=(\eta_1+\sqrt{\tilde{\mu}_1},\eta_2), \tag{48}$$

$$\begin{pmatrix}\eta_1\\ \eta_2\end{pmatrix}=\begin{pmatrix} 0 & 1 \\ \sqrt{2\tilde{\mu}_1} & 0 \end{pmatrix}\begin{pmatrix}z_1\\ z_2\end{pmatrix}, \tag{49}$$

$$\begin{pmatrix}z_1\\ z_2\end{pmatrix}=\begin{pmatrix} 0 & 1/\sqrt{2\tilde{\mu}_1} \\ 1 & 0 \end{pmatrix}\begin{pmatrix}\eta_1\\ \eta_2\end{pmatrix}. \tag{50}$$

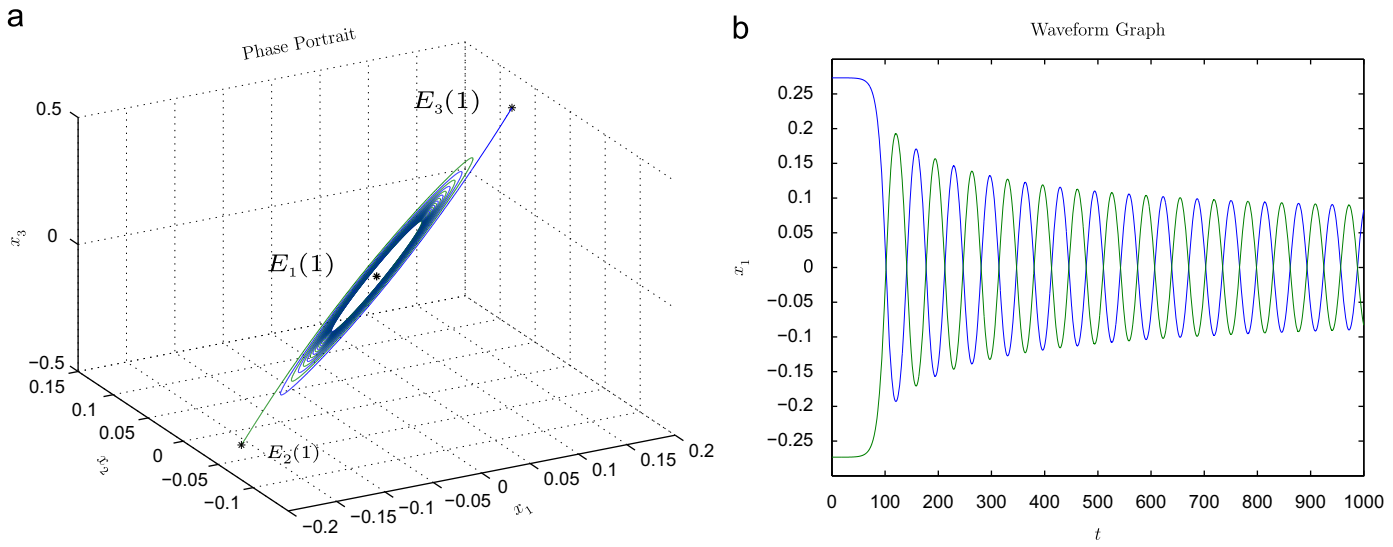

Fig. 6. Numerical results for system (7) in region (III) of Fig. 4a (near the curve $H_{E_1(1)}$) when $(w_1, w_2)=(-0.6,1.33)$. As (w_1, w_2) passes the curve $H_{E_1(1)}$, a stable limit cycle will emerge around $E_1(1)$ and the equilibrium itself becomes unstable; because, on the curve $H_{E_1(1)}$, system (7) undergoes a supercritical Hopf bifurcation at $E_1(1)$. The limit cycle is illustrated in the phase portrait (a) and its corresponding waveform graph (b).

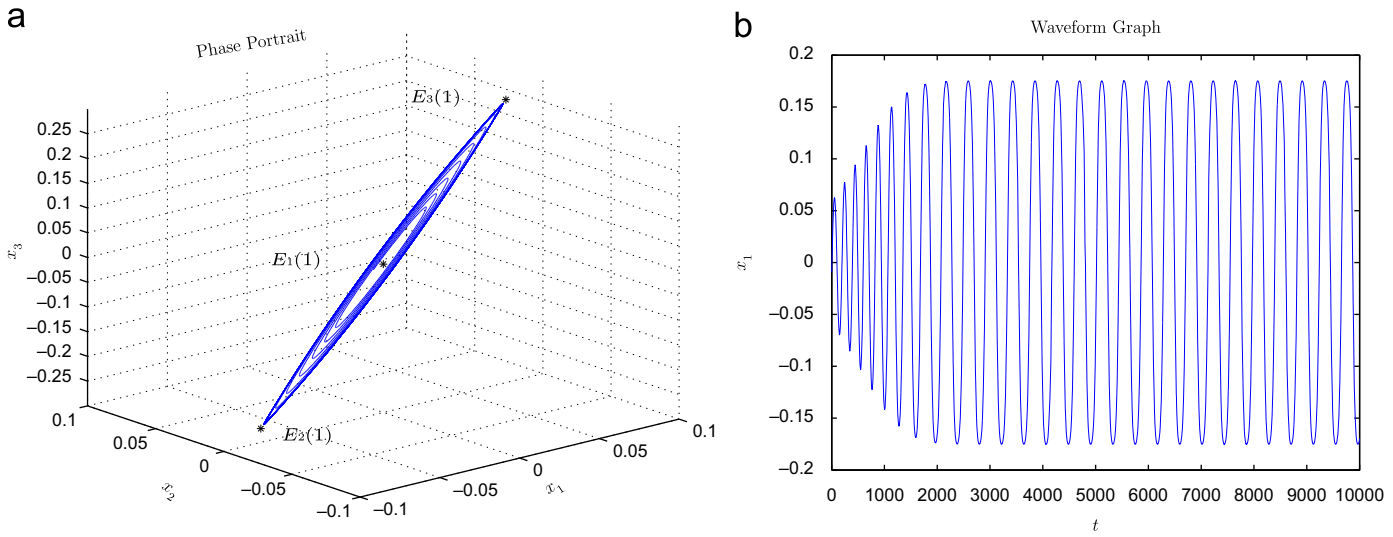

Fig. 7. Numerical results for system (7) in region (III) of Fig. 4a (near the curve $Hetero_{E_{2,3}(1)}$) when $(w_1, w_2)=(-0.6,1.338)$. The phase portrait (a) and its corresponding waveform graph (b) show that as (w_1, w_2) gets closer to the curve $Hetero_{E_{2,3}(1)}$, the limit cycle, generated by the Hopf bifurcation, tends to form a heteroclinic cycle connecting $E_2(1)$ and $E_3(1)$.

If we apply (48)–(50) for small $|\tilde{\mu}_2-\tilde{\mu}_1|$, system (25) will become

$$\begin{cases} \dot{z}_1 = (\tilde{\mu}_2-\tilde{\mu}_1)z_1-\sqrt{2\tilde{\mu}_1}z_2-2\sqrt{\tilde{\mu}_1}z_1z_2-\dfrac{3}{2}\sqrt{2}z_2^2-z_1z_2^2-\dfrac{1}{\sqrt{2\tilde{\mu}_1}}z_2^3, \\ \dot{z}_2 = \sqrt{2\tilde{\mu}_1}z_1. \end{cases} \tag{51}$$

After some calculations, one obtains

$$\frac{d}{d\tilde{\mu}_2}Re\lambda_{1,2}(\tilde{\mu}_2)\Big|_{\tilde{\mu}_2=\tilde{\mu}_1} = \frac{1}{2} \neq 0. \tag{52}$$

By applying the stability formula (41) for

$$F = -2\sqrt{\tilde{\mu}_1}z_1z_2-\frac{3}{2}\sqrt{2}z_2^2-z_1z_2^2-\frac{1}{\sqrt{2\tilde{\mu}_1}}z_2^3, \quad G=0, \quad \text{and}$$
$$\omega = \sqrt{2\tilde{\mu}_1}, \tag{53}$$

one gets

$$Re[c_1(\tilde{\mu}_2)]|_{\tilde{\mu}_2=\tilde{\mu}_1} = \frac{1}{4} > 0. \tag{54}$$

Inequality (54) implies that a generic subcritical Hopf bifurcation occurs in system (25) at $E_3(-1)$; that is, a family of unstable periodic solutions emanates from $E_3(-1)$, as the bifurcation parameter, $\tilde{\mu}_2$, passes its critical value, $\tilde{\mu}_1$.

According to [9], there are two global bifurcation curves in this case, one for a homoclinic bifurcation on which two homoclinic orbits to the origin emerge, and the other for a fold bifurcation for limit cycles on which two limit cycles collide with each other and disappear. The homoclinic bifurcation curve is given by the equation:

$$\tilde{\mu}_2 = \frac{4}{5}\tilde{\mu}_1+\mathcal{O}(\tilde{\mu}_1^2), \tag{55}$$

and the curve of fold bifurcation for limit cycles is given by the equation:

$$\tilde{\mu}_2 = c\tilde{\mu}_1, \tag{56}$$

where $c \approx 0.752$.

Now, by using Eqs. (22) and (26), all bifurcation curves can be illustrated in the (w_1,w_2)-space and as a result, several phase portraits of system (7) can be constructed.

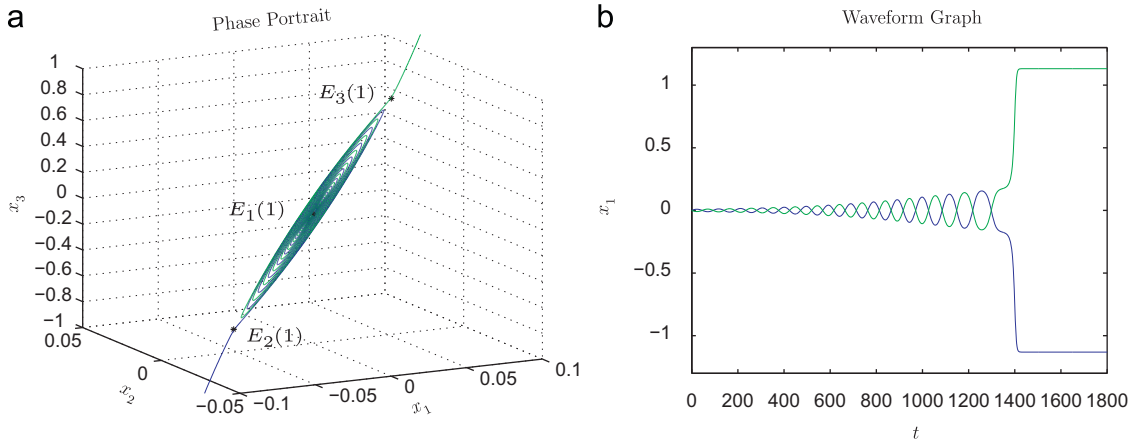

Fig. 8. Numerical results for system (7) in region (IV) of Fig. 4a when $(w_1, w_2)=(-0.6,1.3385)$. As (w_1, w_2) enters region (IV), the two heteroclinic orbits disappear. The phase portrait (a) and the waveform graph (b) show that $E_1(1)$ remains unstable and repels all trajectories nearby including the two stable manifolds of the equilibria $E_2(1)$ and $E_3(1)$.

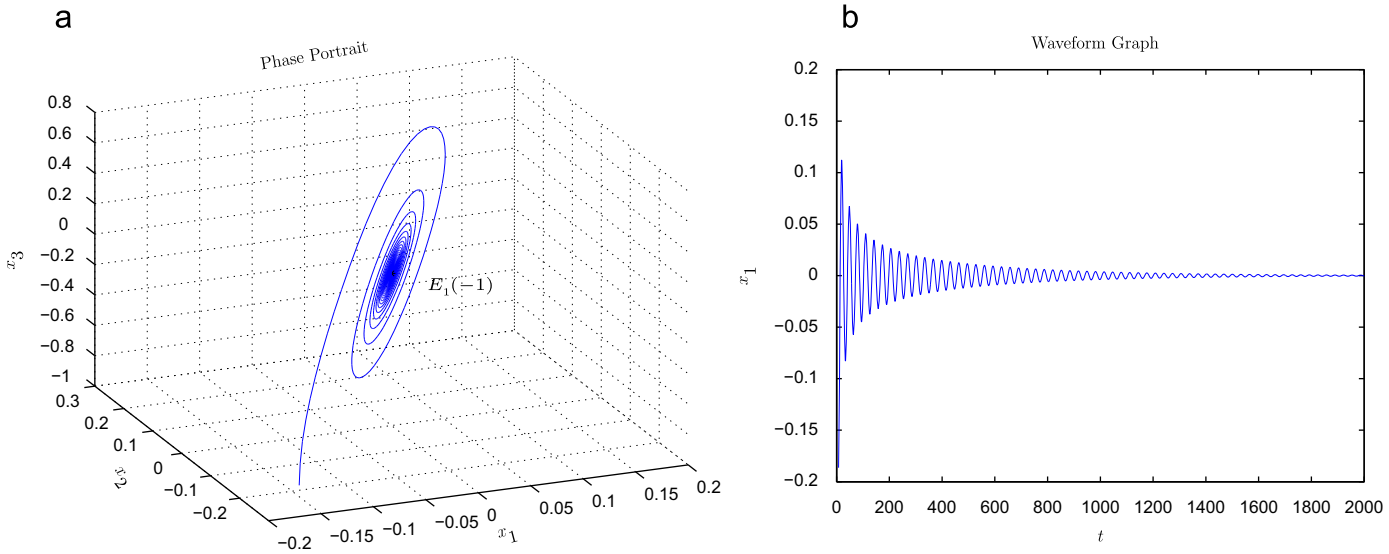

Fig. 9. Numerical results for system (7) in region (I) of Fig. 4b when $(w_1, w_2)=(-16.5,11.8)$. The only equilibrium of the system, $E_1(-1)$, is a stable spiral. This is shown in the phase portrait (a) and its corresponding waveform graph (b).

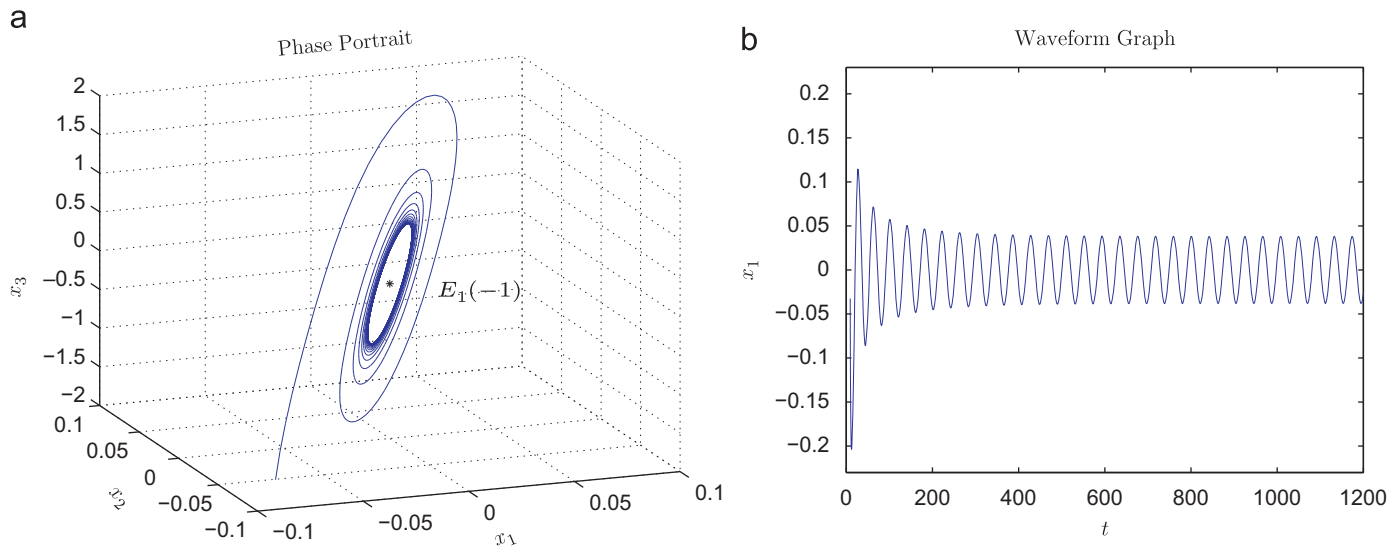

Fig. 10. Numerical results for system (7) in region (II) of Fig. 4b when $(w_1, w_2)=(-16.5,12)$. As (w_1, w_2) crosses the curve $H_{E_1(-1)}$, a stable limit cycle will emerge around $E_1(-1)$ due to the occurrence of a supercritical Hopf bifurcation at $E_1(-1)$ and the equilibrium itself becomes unstable. The limit cycle is illustrated in the phase portrait (a) and its corresponding waveform graph (b).

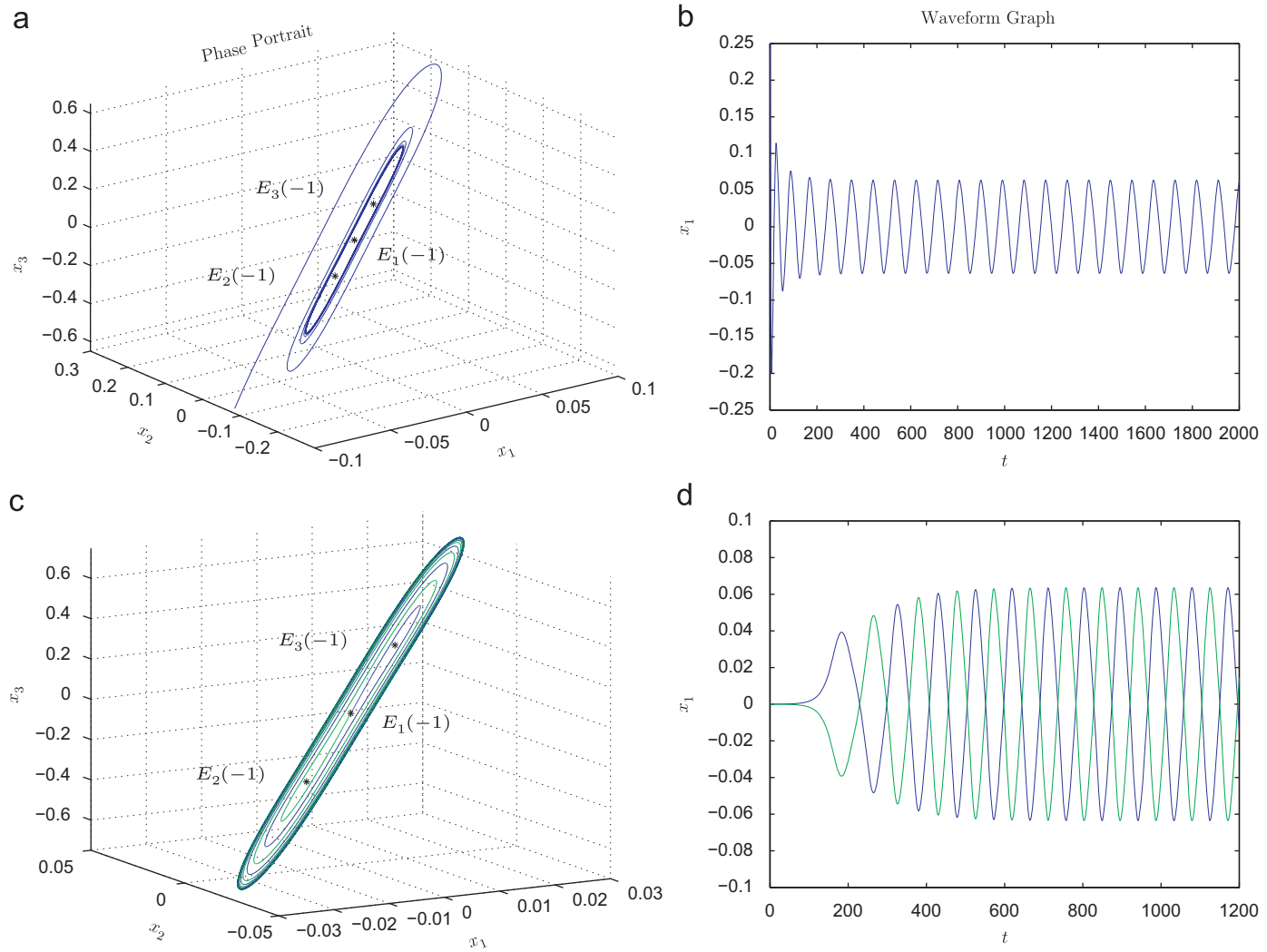

Fig. 11. Numerical results for system (7) in region (III) of Fig. 4b when $(w_1, w_2)=(-16.5,12.265)$. In this region, two nonzero saddles, $E_2(-1)$ and $E_3(-1)$, appear inside the stable limit cycle which is previously generated by the Hopf bifurcation. The phase portrait (a) and its corresponding waveform graph (b) show that all trajectories, starting from an arbitrary point in a neighborhood of the origin outside of the big stable limit cycle, are attracted by the stable limit cycle. The phase portrait (c) and its corresponding waveform graph (d) show the attraction of the two one-dimensional unstable manifolds of the equilibrium $E_1(-1)$ by the stable limit cycle.

4. Bifurcation diagrams and phase portraits

In this section, bifurcation diagrams of two cases $s=1$ and -1 are presented in Fig. 4.

In Fig. 4a, $s=1$ and the transfer function of the neurons is taken as $f(\cdot)=\frac{3}{2}\tanh(\cdot)$; therefore, in Eq. (4) we have $\alpha_1=3/2$ and $\alpha_3=-1/2$. In Fig. 4a, the pitchfork and Hopf bifurcation (at $E_1(1)$) curves are labeled with $P_{E_1(1)}$ and $H_{E_1(1)}$, respectively. Also there is a heteroclinic bifurcation curve, labeled with $Hetero_{E_{2,3}(1)}$, on which system (7) possesses two heteroclinic orbits connecting $E_2(1)$ and $E_3(1)$. Several phase portraits and their corresponding waveform graphs are given in Figs. 5–8 by choosing different values for the parameters in different regions of Fig. 4a. In region (I), system (7) has the unique saddle, $E_1(1)$. As (w_1,w_2) passes the curve $P_{E_1(1)}$, the equilibrium $E_1(1)$ becomes stable and two nonzero equilibria $E_2(1)$ and $E_3(1)$ appear. Fig. 5 depicts the phase portrait and its corresponding waveform graph for the values of parameters in region (II) and close to the Hopf bifurcation curve $H_{E_1(1)}$. As parameters pass $H_{E_1(1)}$, system (7) undergoes a supercritical Hopf bifurcation at $E_1(1)$; therefore, a stable limit cycle emerges around $E_1(1)$ and the equilibrium itself becomes unstable. This can be seen in Fig. 6 for the values of parameters in region (III) and close to the curve $H_{E_1(1)}$. As the two parameters w_1 and w_2 get closer to the curve $Hetero_{E_{2,3}(1)}$, the limit cycle, generated by the Hopf bifurcation, tends to form two heteroclinic orbits connecting $E_2(1)$ and $E_3(1)$. Fig. 7 illustrates the onset of the two heteroclinic orbits formation. Fig. 8 shows that these heteroclinic orbits vanish when parameters take values in region (IV).

In Fig. 4b, $s=-1$ and the transfer function of the neurons is taken as $f(\cdot)=\frac{1}{2}\tanh(\cdot)$; therefore, in Eq. (4) we have $\alpha_1=1/2$ and $\alpha_3=-1/6$. In Fig. 4b, there are one pitchfork bifurcation (at $E_1(-1)$) curve and two Hopf bifurcation (one at $E_1(-1)$ and the other at $E_{2,3}(-1)$) curves which are labeled with $P_{E_1(-1)}$, $H_{E_1(-1)}$ and $H_{E_{2,3}(-1)}$, respectively. Also, there are a homoclinic bifurcation curve, labeled with $Homo_{E_1(-1)}$, on which system (7) has two homoclinic orbits to $E_1(-1)$, and a curve of fold bifurcation for limit cycles which is denoted by *FLC*. In Figs. (9)–(14), several phase portraits and their corresponding waveform graphs are given by choosing different values for the parameters in different regions of Fig. 4b. Fig. 9 shows that in region (I), system (7) has the unique stable spiral $E_1(-1)$. As (w_1,w_2) passes the curve $H_{E_1(-1)}$, system (7) undergoes a supercritical

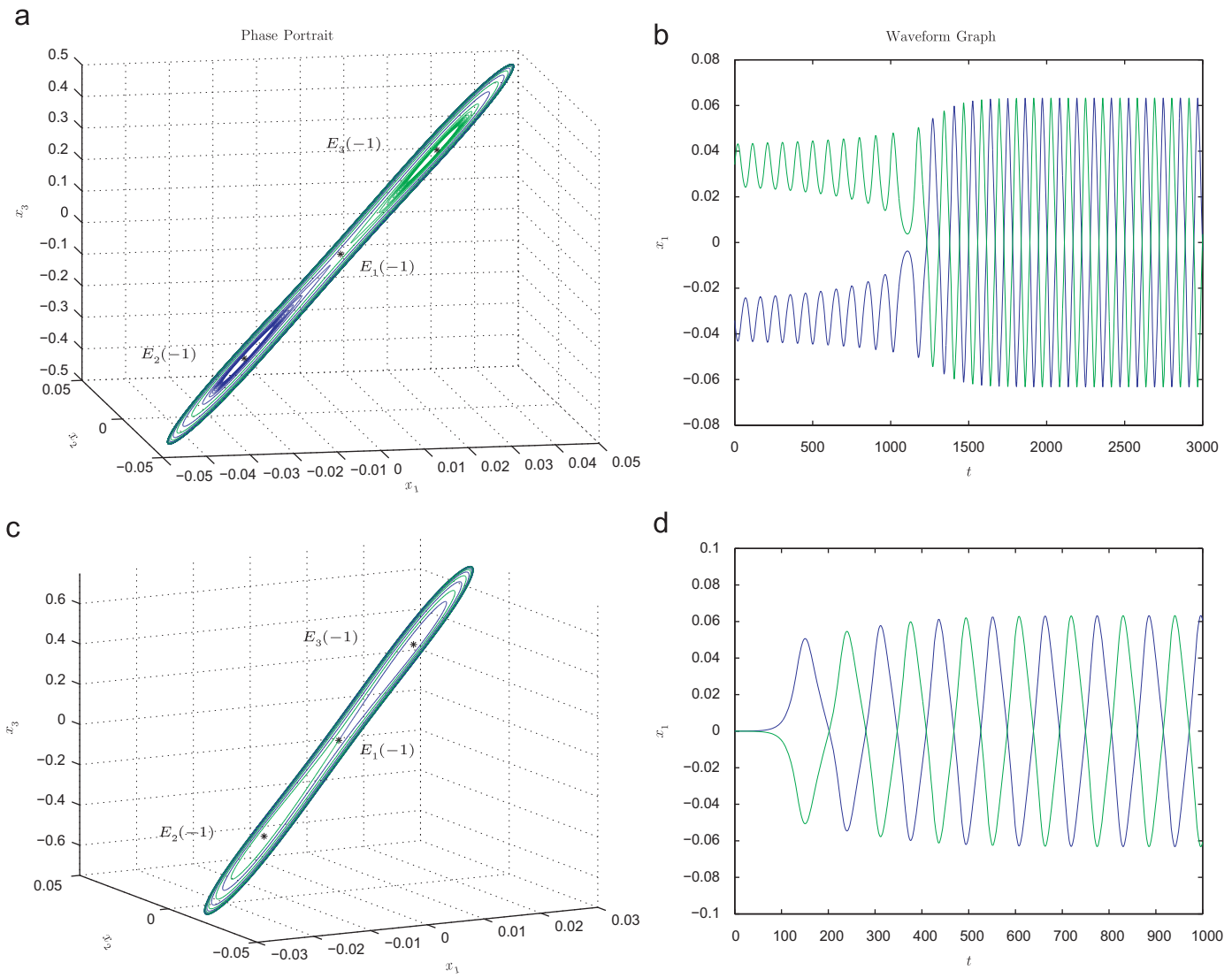

Fig. 12. Numerical results for system (7) in region (IV) of Fig. 4b when $(w_1,w_2)=(-16.5,12.28)$. As (w_1, w_2) passes the curve $H_{E_{2,3}(-1)}$, system (7) simultaneously undergoes a subcritical Hopf bifurcation at $E_2(-1)$ and $E_3(-1)$; as a result, two unstable limit cycles emerge around these two nonzero equilibria and the equilibria themselves become stable. The phase portrait (a) and its corresponding waveform graph (b) show that trajectories, starting from an arbitrary point in a neighborhood of each small unstable limit cycle (outside of the small limit cycles), are attracted by the big stable limit cycle. The phase portrait (c) and its corresponding waveform graph (d) show the attraction of the two one-dimensional unstable manifolds of the equilibrium $E_1(-1)$ by the stable limit cycle.

Hopf bifurcation at $E_1(-1)$; therefore, a stable limit cycle emerges around $E_1(-1)$ and the equilibrium itself becomes unstable. This can be seen in Fig. 10 for the values of the parameters in region (II). As the two parameters w_1 and w_2 cross the curve $P_{E_1(-1)}$ and enter region (III), two nonzero equilibria $E_2(-1)$ and $E_3(-1)$ appear. In Fig. 11, the phase portraits (a) and (c) and their corresponding waveform graphs (b) and (d) illustrate that the stable limit cycle, generated by the Hopf bifurcation, surrounds the three equilibria. Fig. 12 shows that when w_1 and w_2 pass the curve $H_{E_{2,3}(-1)}$ and take their values in region (IV), a subcritical Hopf bifurcation simultaneously takes place at the two nonzero equilibria $E_2(-1)$ and $E_3(-1)$; as a result, two small unstable limit cycles appear around these two equilibria and the equilibria themselves become stable. Fig. 13 shows that as (w_1, w_2) crosses the curve $Homo_{E_1(-1)}$ and enters region (V), not only the two small unstable limit cycles disappear, but also a big unstable limit cycle (not shown in the figure) emerges inside the big stable limit cycle. The phase portraits (a) and (c) and their corresponding waveform graphs (b) and (d) show that trajectories, starting from an arbitrary point in a neighborhood of the origin outside of the big stable limit cycle, will be attracted by the stable limit cycle. Also, all trajectories near $E_2(-1)$ and $E_3(-1)$ are attracted by one of these nonzero equilibria. This, in particular, indicates that the two small unstable limit cycles are eliminated. As the values of parameters are set in region (VI), the two big limit cycles (one stable and the other unstable) disappear as a result of a collision on the curve *FLC*. Fig. 14 indicates that system (7) has no limit cycle in region (VI); therefore, all trajectories, starting from an arbitrary point in a neighborhood of the origin, will converge to one of the two nonzero equilibria.

5. Summary and further work

A three-neuron recurrent neural network has been studied in the neighborhood of the Bogdanov–Takens codimension two bifurcation point where the linear part of the system has a pair of simple zero eigenvalues. It has been shown that if the slope of the

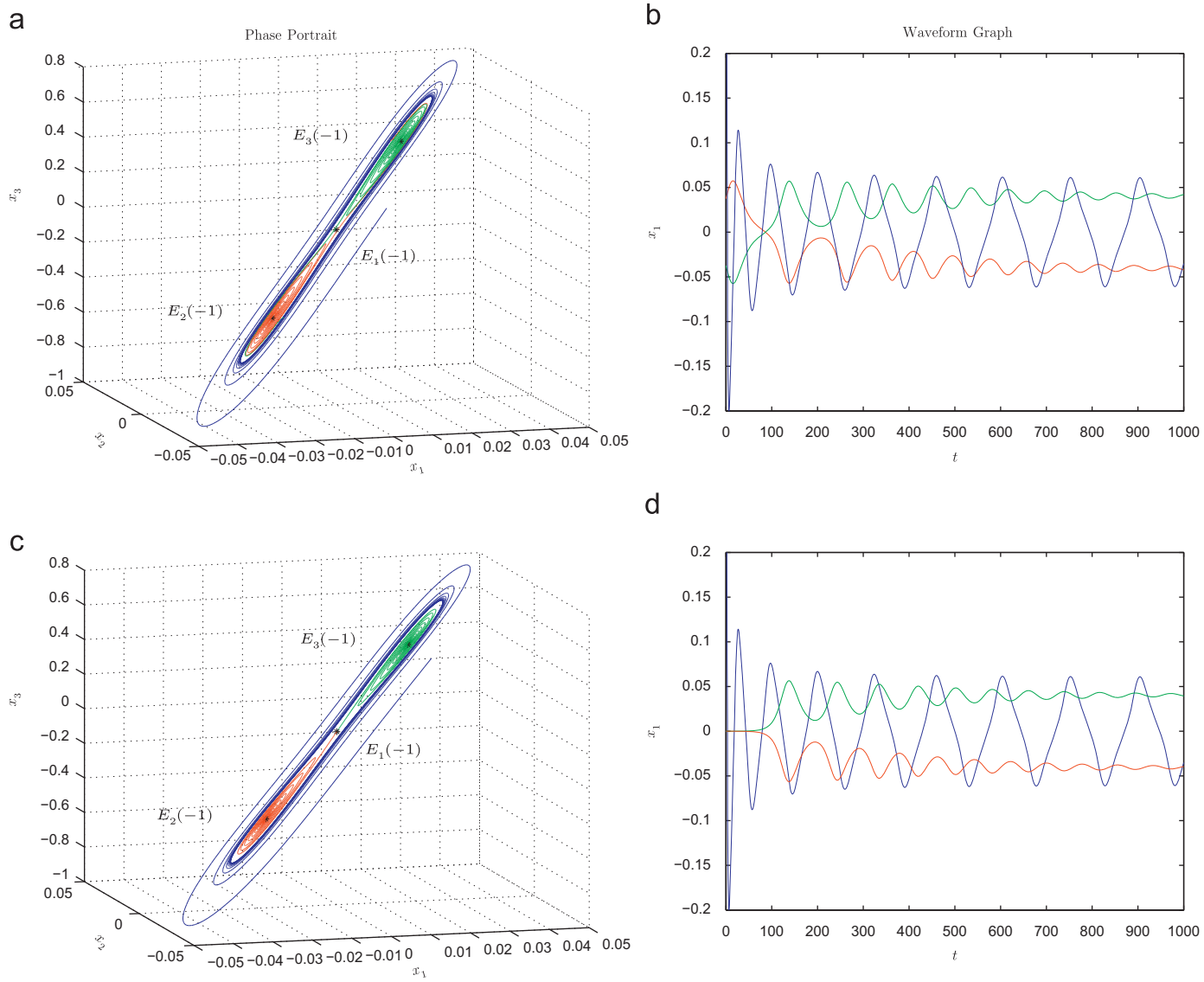

Fig. 13. Numerical results for system (7) in region (V) of Fig. 4b when $(w_1, w_2)=(-16.5,12.29)$. As (w_1, w_2) crosses the curve $Homo_{E_1(-1)}$, not only the two small unstable limit cycles disappear, but also a big unstable limit cycle (not shown in the figure) emerges inside the stable limit cycle. The phase portrait (a) and its corresponding waveform graph (b) show that trajectories, starting from an arbitrary point in a neighborhood of the origin outside of the big stable limit cycle, will be attracted by the stable limit cycle. Also, all trajectories near $E_2(-1)$ and $E_3(-1)$, are attracted by one of these nonzero equilibria; this indicates that the two small unstable limit cycles are eliminated. The phase portrait (c) and its corresponding waveform graph (d) show that the two one-dimensional unstable manifolds of the equilibrium $E_1(-1)$ are attracted by the two nonzero equilibria $E_2(-1)$ and $E_3(-1)$.

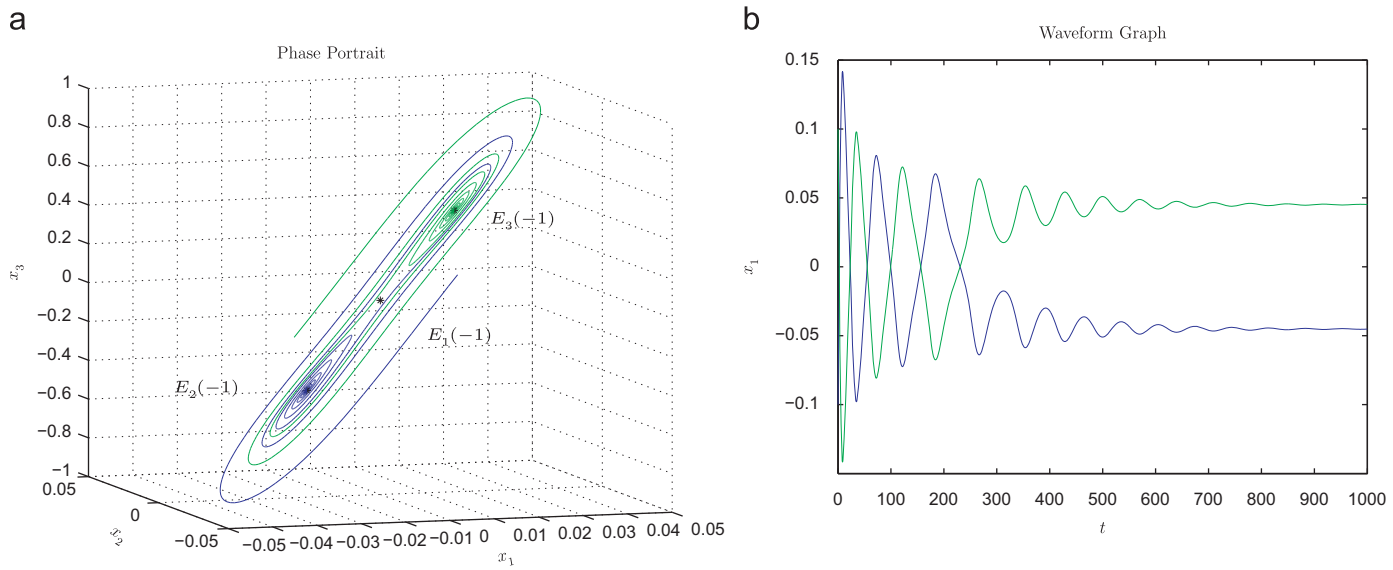

Fig. 14. Numerical results for system (7) in region (VI) of Fig. 4b when $(w_1, w_2) = (-16.5, 12.3)$. As parameters enter this region, the two big limit cycles (one stable and the other unstable) disappear as a result of a collision on the curve *FLC*. In this case all trajectories, starting from an arbitrary point in a neighborhood of the origin, will be trapped in the basin of attraction of one of the two nonzero equilibria. This can be seen for two trajectories in phase portrait (a) and its corresponding waveform graph (b).

transfer function of the neurons at the origin takes positive values other than one, system (7) can be reduced to the Bogdanov–Takens normal form (20) when the two network parameters are fixed at their critical values. By introducing the unfolding parameters, a full investigation has been carried out on system (25) in two different cases. In the first case when $s=1$, that is when $\alpha_1 > 1$, it has been shown that system (25) undergoes a generic pitchfork and a generic supercritical Hopf bifurcation at the origin. It has also been shown that in a specific region in the parameter space where system (25) has three equilibria, there is a curve on which system (25) possesses two heteroclinic orbits connecting the two nonzero equilibria. In the second case when $s=-1$, that is when $\alpha_1 < 1$, it has been shown that in addition to the pitchfork and Hopf bifurcation curves for the origin, there exists a bifurcation curve on which system (25) undergoes a generic subcritical Hopf bifurcation at the two nonzero equilibria. Moreover, the existence of a homoclinic bifurcation curve on which system (25) possesses two homoclinic orbits to the origin, and also a curve of fold bifurcation for limit cycles has been shown. If the slope of the transfer function at the origin is not equal to one, then system (25) will have at most three equilibria and therefore some bifurcation curves presented in [7] will vanish. If the slope at the origin is equal to one, the coefficient of ξ_1^3 will become zero and as a result, we have to consider higher order terms in the normal form of system (7). This suggests that in addition to the two parameters w_1 and w_2, the parameter α_1, introduced in transfer function (4), can be considered as the third bifurcation parameter in the study of system (7). In other words, in the (w_1,w_2,α_1)-space, the point $(w_1^*,w_2^*,\alpha_1^*) = (-2/\alpha_1^3, 3/\alpha_1^2, 1)$ is a codimension three bifurcation point for system (7) at the origin. In this case, the normal form of system (7) contains fifth order terms and its unfolding is provided by the three-parameter family

$$\begin{cases} \dot{\xi}_1 = \xi_2, \\ \dot{\xi}_2 = \mu_1\xi_1 + \mu_2\xi_2 + \mu_3\xi_1^3 + b_3\xi_1^2\xi_2 + a_5\xi_1^5 + b_5\xi_1^4\xi_2, \end{cases} \tag{57}$$

where μ_i $(i=1,2,3)$ are functions of w_i $(i=1,2)$ and α_i $(i=1,3,5,\ldots)$. The investigation of system (57) with three bifurcation parameters is interesting but that is beyond the scope of this paper.

Acknowledgments

The authors wish to thank anonymous referees for their valuable comments which improved this paper.

References

[1] A. Atiya, P. Baldi, International Journal on Neural Systems 1 (1989) 103–124.
[2] J. Cao, D. Huang, Y. Qu, Global robust stability of delayed recurrent neural networks, Chaos, Solitons & Fractals 23 (2005) 221–229.
[3] J. Cao, J. Wang, Absolute exponential stability of recurrent neural networks with Lipschitz-continuous activation functions and time-delays, Neural Networks 17 (2005) 379–390.
[4] B. Chen, J. Wang, Global exponential periodicity and global exponential stability of a class of recurrent neural networks with various activation functions and time-varying delays, Neural Networks 20 (2007) 1067–1080.
[5] M.A. Cohen, S. Grossberg, Absolute stability of global pattern formation and parallel memory storage by competitive neural networks, IEEE Trans. Syst. Man, and Cybernetics SMC-13 (1983) 815–826.
[6] K. Doya, S. Yoshizawa, Adaptive neural oscillator using continuous time back propagation learning, Neural Networks 2 (1989) 375–385.
[7] B. Gao, W. Zhang, Equilibria and their bifurcations in a recurrent neural network involving iterates of a transcendental function, IEEE Transactions on Neural Networks 19 (2008) 782–794.
[8] C.M. Gray, P. Koenig, A.K. Engel, W. Singer, Oscillatory responses in cat visual cortex exhibit inter-columnar synchronization which reflects global stimulus properties, Nature 338 (1989) 334–337.
[9] J. Guckenheimer, P. Holmes, Nonlinear Oscillations, Dynamical Systems and Bifurcations of Vector Fields, Springer-Verlag, New York, 1990.
[10] A. Hajihosseini, G.R. Rokni Lamooki, B. Beheshti, F. Maleki, The Hopf bifurcation analysis on a time-delayed recurrent neural network in the frequency domain, Neurocomputing 73 (2010) 991–1005.
[11] R. Haschke, J.J. Steil, Input space bifurcation manifolds of recurrent neural networks, Neurocomputing 64 (2005) 25–38.
[12] S. Hastings, J. Tyson, D. Webster, Existence of periodic solutions for negative feedback cellular control systems, Journal of Differential Equations 25 (1977) 39–64.
[13] J.J. Hopfield, Neurons with graded response have collective computational properties like those of two-state neurons, Proceedings of the National Academy of Sciences 81 (1984) 3088–3092.
[14] H.K. Khalil, Nonlinear Systems, Prentice-Hall, 1996.
[15] Y.A. Kuznetsov, Elements of Applied Bifurcation Theory, Springer-Verlag, New York, 1998.
[16] C. Lien, L. Chung, Global asymptotic stability for cellular neural networks with discrete and distributed time-varying delays, Chaos, Solitons & Fractals 34 (2007) 1213–1219.

[17] Y. Liu, Z. Wang, X. Liu, Global exponential stability of generalized recurrent neural networks with discrete and distributed delays, Neural Networks 19 (2006) 667–675.
[18] Y. Liu, Z. Wang, A. Serrano, X. Liu, Discrete-time recurrent neural networks with time-varying delays: Exponential stability analysis, Physics Letters A 362 (2007) 480–488.
[19] K. Lu, D. Xu, Z. Yang, Global attraction and stability for Cohen–Grossberg neural networks with delays, Neural Networks 19 (2006) 1538–1549.
[20] J.L. Moiola, G. Chen, Hopf Bifurcation Analysis: A Frequency Domain Approach, World Scientific, Singapore, 1996.
[21] B.A. Pearlmutter, Gradient calculations for dynamic recurrent neural networks: a survey, IEEE Transactions on Neural Networks 6 (1995) 1212–1228.
[22] A.C. Ruiz, D.H. Owens, S. Townley, Existence, learning and replication of periodic motions in recurrent neural networks, IEEE Transactions on Neural Networks 9 (1998) 651–661.
[23] Q. Song, Exponential stability of recurrent neural networks with both time-varying delays and general activation functions via LMI approach, Neurocomputing 71 (2008) 2823–2830.
[24] Q. Song, J. Cao, Z. Zhao, Periodic solutions and its exponential stability of reaction–diffusion recurrent neural networks with continuously distributed delays, Nonlinear Analysis: Real World Applications 7 (2006) 65–80.
[25] Q. Song, Z. Wang, Neural networks with discrete and distributed time-varying delay: a general stability analysis, Chaos, Solitons & Fractals 37 (2008) 1538–1547.
[26] S. Townley, A. Ilchmann, M.G. Weiss, W. Mcclements, A.C. Ruiz, D.H. Owens, D. Praetzel-Wolters, Existence and learning of oscillations in recurrent neural networks, IEEE Transactions on Neural Networks 11 (2000) 205–214.
[27] Z. Wang, Y. Liu, K. Fraser, X. Liu, Stochastic stability of uncertain Hopfield neural networks with discrete and distributed delays, Physics Letters A 354 (2006) 288–297.
[28] Z. Wang, Y. Liu, X. Liu, On global asymptotic stability of neural networks with discrete and distributed delays, Physics Letters A 345 (2005) 299–308.
[29] Z. Wang, H. Shu, J. Fang, X. Liu, Robust stability for stochastic Hopfield neural networks with time delays, Nonlinear Analysis: Real World Applications 7 (2006) 1119–1128.
[30] S. Wiggins, Introduction to Applied Nonlinear Dynamical Systems and Chaos, Springer-Verlag, New York, 2003.
[31] H. Yang, T.S. Dillon, Exponential stability and oscillation of Hopfield graded response neural network, IEEE Transactions on Neural Networks 5 (1994) 719–729.
[32] W. Yu, J. Cao, G. Chen, Stability and Hopf bifurcation of a general delayed recurrent neural network, IEEE Transactions on Neural Networks 19 (2008) 845–854.

F. Maleki is graduated in applied mathematics (M.Sc., Iran, 2009), and is a research assistant in Center of Excellence in Biomathematics at University of Tehran. Her fields of interest are dynamical systems, bifurcation theory, and mathematical neuroscience.

B. Beheshti is graduated in applied mathematics (B.Sc., Iran, 2008), and is a research assistant in Center of Excellence in Biomathematics at University of Tehran. His field of interest is dynamical systems.

A. Hajihosseini is graduated in applied mathematics (M.Sc., Iran, 2007), and is a research assistant in Center of Excellence in Biomathematics at University of Tehran. His fields of interest are dynamical systems, bifurcation theory, and mathematical neuroscience.

G.R. Rokni Lamooki is a lecturer in applied mathematics (Ph.D., UK, 2003), and is a researcher in Center of Excellence in Biomathematics at University of Tehran. His fields of interest are control theory and mathematical biology.